Electrical Transport and Electronic Delocalization of Small Fullerenes

R. Q. Zhang,*,† Y. Q. Feng,‡ S. T. Lee,† and C. L. Bai§

Center of Super-Diamond and Advanced Films (COSDAF) & Department of Physics and Materials Science, City University of Hong Kong, Hong Kong SAR, People's Republic of China, School of Science, Beijing Institute of Technology, Beijing 100081, People's Republic of China, and Nano Science and Technology Center and Institute of Chemistry, Chinese Academy of Science, Beijing 100080, People's Republic of China

Received: May 27, 2004; In Final Form: August 26, 2004

We report the electrical transport properties of several small fullerenes sandwiched between two metallic electrodes and modulated by a gate electrode, calculated using an orthodox theory. The relationship between the charging energies and the structures of fullerenes is obtained. Bond types and molecular curvatures are observed to be important in determining charging energies. The calculated current−voltage and conductance characteristics are related to the electronic structures of fullerenes near energy gaps and are adjustable by the applied gate voltages, indicating that molecular devices with different functions can be designed by selecting fullerenes with proper bond types and curvatures, and by changing the applied gate voltages.

Introduction

As a novel carbon analogue to graphite and diamond, fullerenes, which were discovered 10 years ago, have stimulated great interest among the scientific community. They are hollow cages that consist of 12 pentagonal faces and any number (except 1) of hexagonal faces.[1] In the fullerene family, C_{60} was the first to be discovered in 1985[2] for its rich quantity in solvent-extracted carbon soot. Since then, fullerenes have been extensively researched, for the purpose of producing new materials with promising physical and chemical properties.[3−6] Larger-size fullerenes, such as C_{70}, C_{76}, C_{78}, C_{82}, C_{84}, C_{90}, and C_{96}, have been synthesized in macroscopic quantities.[3] Smaller fullerenes, such as C_{30}, C_{32}, C_{36}, C_{40}, and C_{50}, have also been detected by anion photoelectron spectroscopy and mass spectroscopy.[4] Fullerenes smaller than C_{30} were difficult to isolate, because of the presence of the energetically competitive isomers such as rings, bowls, and sheets. C_{20}, which is topologically the smallest fullerene, has also been prepared but exhibits a very short lifetime,[5] whereas C_{30} is experimentally considered to be the smallest stable fullerene.[6]

Previous studies on small fullerenes have focused on their isolation and stability. Although the experimental evidence suggests that C_{30} is the smallest stable fullerenes, C_{28},[7] C_{24},[8] C_{26},[9] and even C_{20} fullerenes[10] were all theoretically predicted to be energetically favorable. The discrepancy was attributed to insufficient annealing of the specimens and, thus, the experiments possibly were far from equilibrium.[10] Theoretical predictions so far for small fullerenes seem to be strongly dependent on the type of calculation method that was used. For C_{20}, for example, a ring isomer,[11] a cage form,[11,12] and a bowl form[13] were predicted to be favorable respectively by Hartree−Fock, Møller−Plesset second-order perturbation, density functional theory (DFT) with local density approximation, and quantum Monte Carlo calculations.

Previous studies on the electrical transport of fullerenes were concentrated on C_{60}.[14−20] Joachim et al.[14] reported the electrical current as a function of tip displacement toward the C_{60} molecule, as measured by scanning tunneling microscopy (STM). It was found that the contact of the STM tip compressed and deformed the C_{60} molecule, leading to the enhancement of conductivity. Meanwhile, an apparent elastic resistance of 54.80 MΩ was given for a single C_{60} molecule. C_{60} was used to make a single-molecule electromechanical amplifier,[15] in which the tunneling between the C_{60} and the tip was modulated by the deformation of C_{60}, and a gain as high as 40 was expected. Porath and co-workers[16,17] measured the discrete tunneling spectra of C_{60}. The rich structures of the current−voltage ($I-V$) spectra indicated a Coulomb blockade and resonant tunneling through the discrete levels and charging effects. Park et al.[18] fabricated single-C_{60} transistors with bias and gate electrodes, and found an obvious Coulomb blockade from the $I-V$ and differential conductivity characteristics. They also proposed a new mechanism of coupling of the center-of-mass motion of C_{60} with a single-electron hopping to describe the special excitation involved. Palacios et al.[19] studied theoretically C_{60} that was well-connected to aluminum electrodes by a Green function technique that combines density functional calculation with a tight binding model. A self-energy matrix was introduced into the Green function to simulate a bulk electrode with several metallic atoms. It was thought that the stronger hybridization of C_{60} with electrodes would provide more channels for the electronic transport. Approximately 3.0 extra electrons were found in C_{60}. Using a similar theory, Taylor et al.[20] investigated a similar system, but with a gate control. They revealed that a gate voltage could change the transmission channels significantly and switch the charge transfer on or off. The aforementioned works indicate that the conduction of C_{60} can be influenced by the deformation of C_{60}, charge transfer from the electrodes to C_{60}, the applied gate voltage, etc. Only the factor of gate voltage can have a role in the tunnel process with longer distances between C_{60} and electrodes.

To our knowledge, the transport of fullerenes smaller than C_{60} has not been investigated experimentally, perhaps because

* Author to whom correspondence should be addressed. Telephone: 852 2788 7849. Fax: 852 2788 7830. E-mail address: aprqz@cityu.edu.hk.
† City University of Hong Kong.
‡ Beijing Institute of Technology.
§ Chinese Academy of Science.

10.1021/jp047698d CCC: $27.50
Published on Web 09/30/2004

of their difficulty in synthesis and isolation. Because the small fullerenes show significant differences in surface curvatures and thus in electronic structures, their study can enhance the understanding of transport properties, in relation to the electronic and structural features and facilitate the development of molecular devices with new functions. Toward this purpose, we systematically explore the transport properties of C_{20}, C_{24}, C_{28}, C_{30}, C_{32}, and C_{60} fullerenes in this work.

Theoretical Formalism and Models of Fullerenes

A fullerene molecule, as shown in Figure 1a, is weakly coupled between two bias electrodes through vacuum tunnel barriers. The electrical transport is described statistically by subsequent electron tunneling through the electrode−fullerene−electrode junctions, modulated by a gate voltage. The gate voltage is expected to control the electrostatic potential of the fullerene without causing a current flow between the fullerene and the gate.

Each of the discrete single electronic levels ϵ_i of the small-size fullerene may be occupied by either one or zero electron. When an extra electron joins, a charge state is formed, which increases the electrostatic energy by the charging energy $E_c = e^2/(2C)$, where C is the capacitance of the fullerene to all electrodes. Under a gate voltage V_g, the total energy increase due to the joining of N extra electrons to the unoccupied levels is described by[21]

$$E_N = \sum_{i=1}^{N} \epsilon_i + \frac{(Ne)^2}{2C} - \alpha N e V_g \qquad (1)$$

The corresponding chemical potential would be

$$\mu_N = E_N - E_{N-1} = \epsilon_N + (2N-1)E_c - \alpha e V_g \qquad (2)$$

where α is the ratio of the gate capacitance to C. The energy spectra ϵ_i were obtained by performing calculations with a B3LYP method of density functional theory using a Gaussian 98 package.[22] A 3-21G basis set was used. All the fullerenes were geometrically optimized.

Both gold electrodes possess continuum states and can provide electrons to the fullerenes as reservoirs. Their chemical potentials change with the bias voltage (V_b)

$$\mu_F^l = E_F + (1-\eta)eV_b$$
$$\mu_F^r = E_F - \eta e V_b \qquad (3)$$

where E_F is the Fermi energy level without the bias and η is a parameter that is related to the strength of coupling of the fullerene to both electrodes and characterizes the voltage drop over both junctions. The parameter η is assumed, in this work, to be dependent only on the junction width, i.e., $\eta = d_r/(d_l + d_r)$. This assumption is only valid in the weak coupling case (wide barriers) considered here. The tunneling processes from the fullerene to the electrodes or in the reverse direction are considered to be elastic; only the electrons with a chemical potential μ_N could be transported between both electrodes.[21] After an unoccupied level of the fullerene is located between μ_F^l and μ_F^r, a current is induced in the transport channel (see Figure 1b). The calculation details of the current have been described in our previous papers.[23]

All of the fullerene molecules considered in this work are shown in Figure 2, including a C_{20}, a C_{24}, a C_{28}, a C_{30}, a C_{32}, and a C_{60}. They each were placed between the electrodes for their transport property studies.

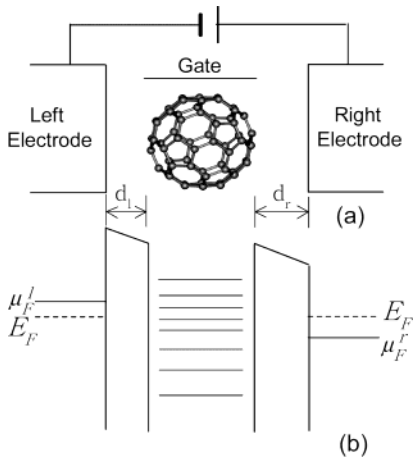

Figure 1. (a) Schematic diagram of a fullerene molecule weakly coupled between two electrodes through vacuum tunnel barriers. (b) Schematic diagram of the energy levels of the fullerene and the bias-induced energy band of the metallic electrodes.

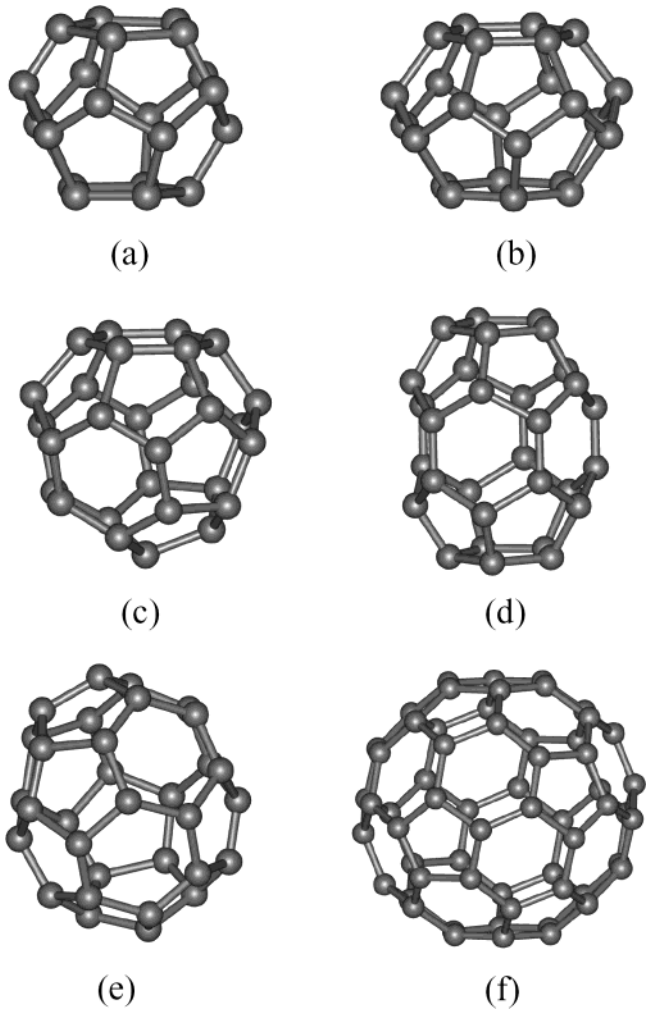

Figure 2. Fullerene molecules considered in this work: (a) C_{20}, (b) C_{24}, (c) C_{28}, (d) C_{30}, (e) C_{32}, and (f) C_{60}.

Results and Discussion

A. Charging Energies. Equation 2 shows that the charging energy has a key role in determining the chemical potential, and then the electrical transport, of fullerenes. The extra

TABLE 1: Charging Energies E_c of the Fullerenes for $N = 1$, Determined from Calculations of Electronic Structures[a]

fullerene	$E_{LUMO}(0)$ (eV)	$E_{HOMO}(1)$ (eV)	E_c (eV) calculated	E_c (eV) scaled	energy gap (eV)
C_{20}	−3.656	−0.529	1.563	0.312	1.858
C_{24}	−4.247	−1.083	1.582	0.316	1.920
C_{28}	−4.698	−1.770	1.464	0.293	1.371
C_{30}	−4.233	−1.324	1.454	0.291	1.382
C_{32}	−4.119	−1.412	1.353	0.271	2.592
C_{60}	−3.567	−1.183	1.192	0.238	2.943

[a] The corresponding energy gaps are also included.

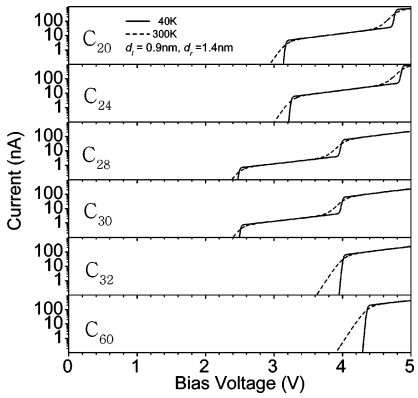

Figure 3. Current−voltage ($I-V$) curves of the fullerenes at 40 and 300 K, without gate voltages.

electrons entering a nanostructure would fill up empty energy levels possibly with some relaxation. It can be expressed as the change of an energy level before and after being occupied by an extra electron:[24]

$$E_c = \frac{\epsilon_{HOMO}(N) - \epsilon_{LUMO}(N-1)}{2} \qquad (\text{for } N = 1, 2, ...) \quad (4)$$

where $\epsilon_{LUMO}(N-1)$ and $\epsilon_{HOMO}(N)$ are respectively the lowest unoccupied level of the fullerenes with $N-1$ extra electrons and the highest occupied level of the fullerenes with N extra electrons. Using eq 4, we calculated the E_c value of the fullerenes for $N = 1$ from the calculation of electronic structures, and the data were listed in Table 1. The calculated E_c value of C_{60} (1.19 eV) is significantly larger than that obtained by fitting to the experimental current−voltage results of adsorbed C_{60} by scanning tunneling spectroscopy (STS), which was only 0.35 or 0.20 eV.[17] The large difference is considered to be mainly due to (i) the deficiency in predicting the energy levels using the hybrid B3LYP theory[22] and (ii) the fact that the measured system involves considerable interactions between C_{60} and the metallic electrodes. Direct calculations of E_c using ab initio theory are difficult for the fullerene−electrode interaction systems. To include the fullerene−electrode interaction in our calculations, for a better comparison of the calculated transport characteristics with experimental results, we scaled the E_c value calculated with eq 4 by a factor of 0.20 (estimated by referencing to the C_{60} data). The scaled values of E_c are shown in Table 1 and will be used in the calculation of the $I-V$ curves and conductance spectra.

B. Transport Characteristics. 1. Current−Voltage Characteristics. Having obtained the E_c value of the fullerenes, we calculated their $I-V$ curves with single-electronic levels. The curves at two temperatures are shown in Figure 3 without a gate voltage. When smaller bias voltages are applied across the two electrodes, the currents are inhibited, indicating that a Coulomb blockade is occurring. Until the bias voltages increase to a critical value, finite currents exist. Here, the LUMO level enters the energy region between the chemical potentials of the two electrodes, creating a transport channel of electrons between the electrodes and the fullerene. The forbidden ranges provide information about the charging energies and band gaps of the fullerenes.[23] The larger this range, the wider the gap. The relative widths of the forbidden ranges are closely related to the energy gaps determined by the B3LYP calculation as listed in the last column of Table 1. It is seen that C_{28} has the smallest energy gap and the smallest forbidden range, whereas C_{60} has the largest values.

At lower temperature, the currents increase sharply around the critical bias, whereas at higher temperature, thermal effects can smear the sharp increase. The Coulomb blockade and the smearing effects have been demonstrated for nanotube fragments in our earlier calculations.[23] However, the threshold voltages here are basically wider than those for the nanotubes, because of the relatively wider HOMO−LUMO gaps. With the bias voltages increasing, current plateaus appear, and the widths of the plateaus are proportional to the charging energy of the fullerenes. At the ends of the plateaus, a second transport channel is opened and the currents undertake another sharp increase, which, afterward, is followed by new plateaus. Such a current rising is called a Coulomb staircase.

The Coulomb staircase cannot always continue, and the currents will decrease when the bias voltages exceed some values, as discussed in our previous work.[23] Therefore, only a few stairs and energy levels are exhibited in the $I-V$ curves, and less information about the electronic structures of fullerenes is expressed. By shifting the energy spectra upward, using gate voltages, more energy levels can be determined.

It has been revealed that electron transport in a nanostructure is very sensitive to the way of applying a bias.[23,25] For this reason, $d_l = 0.9$ nm and $d_r = 14.0$ nm were selected in the above-described calculations, as the Coulomb staircase only exists for the case of $d_l < d_r$.[23] Because the transmission coefficient of the left junction is bigger than that of the right junction, under a moderate bias, the transport bottleneck is the right barrier. As soon as an electron tunnels out of the tube through the right junction, the fullerene is immediately replenished through the left junction. In other words, the fullerene always fills with electrons that can be offered to the right electrode. In contrast, if $d_l > d_r$, the transmission coefficient of the left junction is smaller than that of the right junction, and the transport bottleneck is the left junction.

2. Conductance Characteristics. Differential conductance (dI/dV_b) is often expressed as a function of the bias voltage V_b and gate voltage V_g, as shown in the corresponding gray plots in Figure 4 for C_{60} as an example. The white lines indicate large current (high conductance), black regions mean no current, and the gray regions are intermediate transitions from low conductance to high conductance. When the bias voltage is smaller, a series of black triangular regions can be observed for different gate voltages. Although there may be extra electrons in the fullerene (the numbers are marked in the figure), they are restricted there and cannot induce conductance. The outside electrons are also inhibited from joining the fullerene. Therefore, the bias voltage at the threshold current can be adjusted by the gate voltage. More plateau regions may also be revealed in the $I-V$ curves in this way. The thermal effects on the transport can also be observed in Figure 4. When the temperature increases, the straight lines become thick and the black/white transition is blurred, as shown in the lower figure of Figure 4. This implies that the fullerene becomes conducting as the

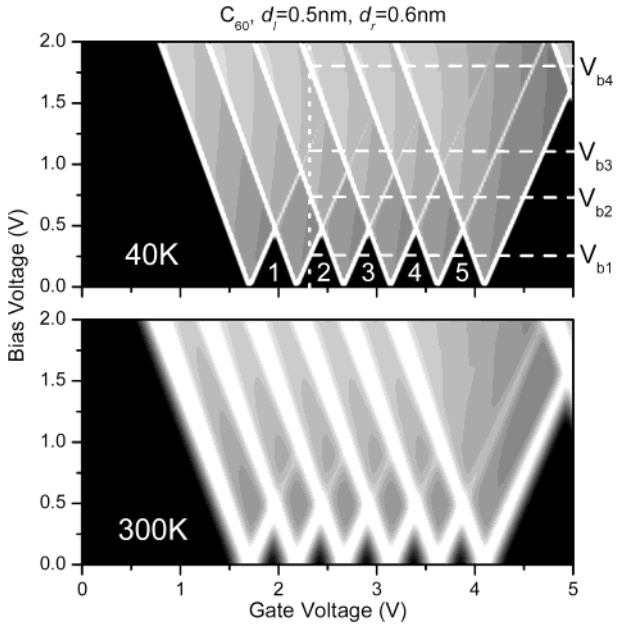

Figure 4. Differential conductance (dI/dV_b), as a function of bias voltage V_b and gate voltage V_g, using C_{60} as an example. White lines indicate large current (high conductance), black regions denote a block of current, and the gray regions represent intermediate conductance.

temperature increases. In other words, the Coulomb blockade is suppressed by the thermal effect.

If the bias is set to zero, several conductance resonance positions can be observed with increasing gate voltage, and these positions indicate the spectrum of chemical potentials of the fullerene. Obviously, the distances between neighboring positions are the same for the first six positions. This can be explained by the three degenerated LUMO levels of C_{60} and their spin degenerate. The distances are twice the E_c value of C_{60}. With increasing gate voltage, the seventh resonance position occurs, and the distance from the sixth resonance to the seventh resonance is equal to $2E_c$ plus the energy separation between LUMO and LUMO+1. For other fullerenes, there exists at least a spin degenerate in their LUMO levels. Thus, a distance of at least $2E_c$ can be observed in the gray plots for zero bias.

When the bias voltage increases, every resonance position emits two resonance lines: one has a negative slope, and the other has a positive slope. According to Figure 1b, the μ_F^l and μ_F^r values are separated from E_F value in the reverse directions for a bias voltage. Only the states with chemical potentials between μ_F^l and μ_F^r can act as the channels for electrons to transport from the left electrodes to the right electrodes. The negatively sloped lines result from the introduction of channels from the region above the μ_F^l level, whereas the positive-sloped lines are from the region below the μ_F^r level. The lines of each type are parallel to each other. For the negatively sloped lines, the thickness is unchanged, indicating that the channels that are opened from the μ_F^l direction can always have a role in inducing the conductance resonance. On the other hand, the positively sloped lines become thinner and darker with increasing bias voltage and even disappear in the gray background. This means that it is difficult to enhance the conductance by a channel newly opened from the μ_F^r direction for bigger bias voltages. The difference between the two types of transport electrons is more apparent if the difference between the left and right junction widths is larger.

From the conductance gray plots, the transport properties of the fullerene can be obtained easily for any bias and gate voltages (V_b and V_g, respectively). Taking $V_g = 2.35$ eV as an example, when $V_b < V_{b1}$, there exist two energy levels below the μ_F^r level; in each of these energy levels, one electron is restricted by the gate voltage, which does not induce conductance. As the bias increases over V_{b1}, the higher of the two energy levels, as a channel, shifts upward to the region between μ_F^l and μ_F^r, allowing an electron to take part in the transport. However, the number of extra electrons is not increased: it remains two. When the bias is increased over V_{b2}, a new channel enters between μ_F^l and μ_F^r from the region above them. This channel does not belong to those originally electron-occupied, and, hence, a transporting electron is introduced, resulting in three extra electrons in the fullerene. Continually raising the bias above V_{b3}, another electron that was originally restricted becomes transporting, but its contribution to conductance is small (still three extra electrons). At a bias voltage over V_{b4}, all four extra electrons participate in the transport. It was reported that the number of extra electrons held in a C_{60} is just three in an equilibrium that is due to the repulsion between electrons.[19,20]

The feature of triangular Coulomb blockade regions has been observed in many transport measurements.[18] However, with some extra indistinct high-conductance lines outside the triangular regions, the experimental gray plots are not as explicit as those shown in Figure 4. This has been known to result from some C_{60}−anion excited states, which are open as channels. In the present work, the fullerenes are assumed to relax fast from excited to ground states, so that they are not involved in those complex structures in the gray plots. Besides, the conductance spectra may present other quantum characteristics of fullerenes (vibration,[18] electronic correlation,[26] etc.).

C. Electronic Delocalization. By measuring the conductance spectra in the experiment, as we demonstrate here using computational data, one may determine the charging energies of fullerenes and then systematically study the relation of the E_c value of fullerenes with their structures. As observed in Table 1, E_c decreases as the atomic numbers of fullerenes decrease, except for C_{20}, which does not possess any hexagonal face. As illustrated below, the trend is closely related to the number of hexagonal faces in the fullerenes. When an electron joins a fullerene, it distributes around the atoms or the bonds. The different bonds should have different capabilities of collecting electrons. The bonds in fullerenes can be simply divided into three types, which are classified according to their neighboring pentagonal and hexagonal faces (see the structures in Figure 2). The first type is the bond shared by two pentagonal faces (denoted as "PP"); the second is shared by a pentagonal face and a hexagonal face (denoted as "PH"); and the third is shared by two hexagonal faces (denoted as "HH"). We used three parameters—C_{PP}, C_{PH}, and C_{HH}—to represent the contributions of the three types of bonds to the E_c value, and we used a function $f = \sum_\alpha C_\alpha n_\alpha$ to fit the E_c values. Here, α denotes PP, PH, and HH, and n_α is the fraction of a type of bonds in a fullerene. The calculated and fitted E_c values are shown in Figure 5. The parameters obtained are $C_{PP} = 0.318$ eV, $C_{PH} = 0.283$ eV, and $C_{HH} = 0.147$ eV, respectively, with a root-mean-square (rms) error of ± 0.006 eV. The relative quantity of the parameters indicates that the PP bonds have the largest contribution to the E_c value, whereas the HH bonds possess the smallest effects, with the PH bonds as the intermediate. In other words, the difficulty for the bonds to accept extra electrons decreases according to the following order: PP, PH, and HH.

This result implies that hexagonal faces accept extra electrons more easily than pentagonal ones, which can be explained in terms of the delocalization degree of electrons in the ring

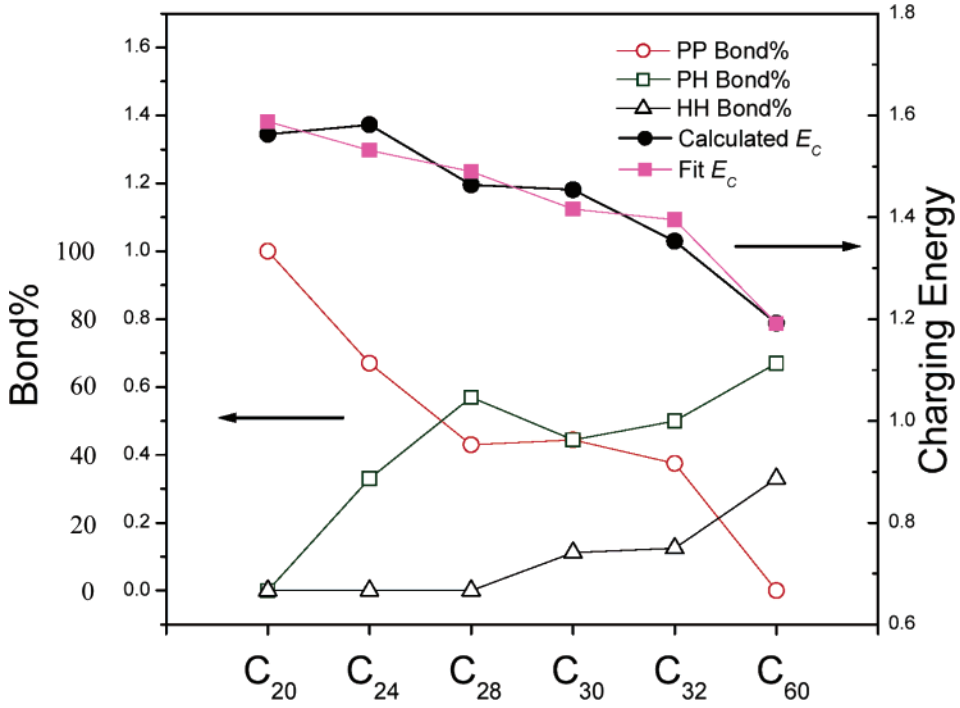

Figure 5. Bond percentages and the calculated and fitted E_c values. The three bond types are denoted by "PP" (the bond shared by two pentagonal faces), "PH" (the bond shared by a pentagonal face and a hexagonal face), and "HH" (the bond shared by two hexagonal faces).

structure.[1,27] As is well-known, there is a large π-bond that connects six C atoms in the benzene (six-membered) ring. The valence electrons can move freely in the ring with strong delocalization and, thus, could accept extra electrons more easily. However, in a five-membered ring, the situation is reversed, because of the lack of conjugated electron. In refs 1 and 27, the delocalization degree of electrons in a ring structure was evaluated by the nucleus-independent chemical shift (NICS), which is relevant to the magnetism of the molecule. Bigger NICS values were found for the pentagonal faces in the fullerenes, indicating stronger localization. When the bonds are neighboring to hexagonal faces, the NICS values decrease; and the higher the number of neighboring hexagonal faces, the more the NICS values decrease. Our fitted results are consistent with these results.

Note that the fitted E_c value does not always compare well with the value calculated directly for some fullerenes, as the above-mentioned fittings only included the main features of bond types. As shown in Figure 5, for C_{20}, C_{28}, and C_{60}, the differences between the fitted and the calculated E_c values are less than those for C_{24}, C_{30}, and C_{32}. As observed from Figure 2, the former group of fullerenes is of a spherical shape, whereas the latter group of fullerenes is ellipsoid-like. This suggests that the charging effects of fullerenes are also related to their shapes.

Summary

In the present work, we studied the electronic transport properties of small fullerenes sandwiched between two metallic electrodes and modulated by a gate electrode. The charging energies were calculated as an important factor that influences their transport. We also investigated the relationship between the charging energies and the structures of fullerenes and revealed that the bond types and molecular shapes are important in determining the charging energies and, thus, the transport properties. The calculated current−voltage and conductance characteristics were shown to relate to the electronic structures of fullerenes near the energy gaps and can be adjusted by the applied gate voltages. The results suggest that one may design molecular devices with different functions by selecting fullerenes with different shapes and bond types, and by changing the applied gate voltages.

Acknowledgment. The work described in this paper is supported by grants from the Research Grants Council of the Hong Kong Special Administrative Region (Project Nos. CityU 3/01C and CityU 1138/02P), CAS-Croucher Funding Scheme for Joint Laboratories and Chinese Academy of Sciences, China.

References and Notes

(1) Chen, Z. F.; Jiao, H. J.; Bühl, M.; Hirsch, A.; Thiel, W. *Theor. Chem. Acc.* **2001**, *106*, 352. Bühl, M.; Hirsch, A. *Chem. Rev.* **2001**, *101*, 1153.

(2) Kroto, H. W.; Heath, J. R.; O'Brien, S. C.; Curl, R. F.; Smalley, R. E. *Nature* **1985**, *318*, 162.

(3) Scuseria, G. E. *Science* **1996**, *271*, 942 and references therein.

(4) Kietzmann, H.; Rochow, R.; Ganteför, G.; Eberhardt, W.; Vietze, K.; Seifert, G.; Fowler, P. W. *Phys. Rev. Lett.* **1998**, *81*, 5378 and references therein.

(5) Prinzbach, H.; Weller, A.; Landenberger, P.; Wahl, F.; Wörth, J.; Scott, L. T.; Gelmont, M.; Olevano, D.; Issendorff, B. V. *Nature* **2000**, *407*, 60.

(6) Radi, P. P.; Bunn, T. L.; Kemper, P. R.; Molchan, M. E.; Bowers, M. T. *J. Chem. Phys.* **1987**, *88*, 2809. Kroto, H. W. *Nature* **1987**, *329*, 529.

(7) Martin, J. M. L. *Chem. Phys. Lett.* **1996**, *255*, 1.

(8) Jensen, F.; Koch, H. *J. Chem. Phys.* **1998**, *108*, 3213.

(9) Kent, P. R. C.; Towler, M. D.; Needs, R. J.; Rajagopal, G. *Phys. Rev. B* **2000**, *62*, 15394.

(10) Taylor, P. R.; Bylaska, E.; Weare, J. H.; Kawai, R. *Chem. Phys. Lett.* **1995**, *235*, 558.

(11) Parasuk, V.; Almlöf, J. *Chem. Phys. Lett.* **1991**, *184*, 187. Feyereisen, M.; Gutowski, M.; Simons, J.; Almlöf, J. *J. Chem. Phys.* **1992**, *96*, 2926.

(12) Brabec, C. J.; Anderson, E. B.; Davidson, B. N.; Kajihara, S. A.; Zhang, Q. M.; Bernholc, J.; Tomanek, D. *Phys. Rev. B* **1992**, *46*, 7326. Raghavachari, K.; Strout, D. L.; Odom, G. K.; Scuseria, G. E.; Pople, J. A.; Johnson, B. G.; Gill, P. M. W. *Chem. Phys. Lett.* **1993**, *214*, 357.

(13) Grossman, J. C.; Mitas, L.; Raghavachari, K. *Phys. Rev. Lett.* **1995**, *75*, 3870. Sokolova, S.; Lüchow, A.; Anderson, J. B. *Chem. Phys. Lett.* **2000**, *323*, 229.

(14) Joachim, C.; Gimzewski, J. K.; Schlittler, R. R.; Chavy, C. *Phys. Rev. Lett.* **1995**, *74*, 2102.

(15) Joachim, C.; Gimzewski, J. K. *Chem. Phys. Lett.* **1997**, *265*, 353. Joachim, C.; Gimzewski, J. K.; Tang, H. *Phys. Rev. B* **1998**, *58*, 16407.
(16) Porath, D.; Millo, O. *J. Appl. Phys.* **1997**, *81*, 2241.
(17) Porath, D.; Levi, Y.; Tarabiah, M.; Millo, O. *Phys. Rev. B* **1997**, *56*, 9829.
(18) Park, H.; Park, J.; Lim, A. K. L.; Anderson, E. H.; Alivisatos, A. P.; McEuen, P. L. *Nature* **2000**, *407*, 57.
(19) Palacios, J. J.; Pérez-Jiménez, A. J.; Louis, E.; Vergés, J. A. *Nanotechnology* **2001**, *12*, 160.
(20) Taylor, J.; Guo, H.; Wang, J. *Phys. Rev. B* **2001**, *63*, 121104.
(21) Beenakker, C. W. J. *Phys. Rev. B* **1991**, *44*, 1646.
(22) Frisch, M. J.; Trucks, G. W.; Schlegel, H. B.; Scuseria, G. E.; Robb, M. A.; Cheeseman, J. R.; Zakrzewski, V. G.; Montgomery, J. A., Jr.; Stratmann, R. E.; Burant, J. C.; Dapprich, S.; Millam, J. M.; Daniels, A. D.; Kudin, K. N.; Strain, M. C.; Farkas, O.; Tomasi, J.; Barone, V.; Cossi, M.; Cammi, R.; Mennucci, B.; Pomelli, C.; Adamo, C.; Clifford, S.; Ochterski, J.; Petersson, G. A.; Ayala, P. Y.; Cui, Q.; Morokuma, K.; Malick, D. K.; Rabuck, A. D.; Raghavachari, K.; Foresman, J. B.; Cioslowski, J.; Ortiz, J. V.; Stefanov, B. B.; Liu, G.; Liashenko, A.; Piskorz, P.; Komaromi, I.; Gomperts, R.; Martin, R. L.; Fox, D. J.; Keith, T.; Al-Laham, M. A.; Peng, C. Y.; Nanayakkara, A.; Gonzalez, C.; Challacombe, M.; Gill, P. M. W.; Johnson, B. G.; Chen, W.; Wong, M. W.; Andres, J. L.; Head-Gordon, M.; Replogle, E. S.; Pople, J. A. *Gaussian 98*, revision A.7; Gaussian, Inc.: Pittsburgh, PA, 1998.
(23) Feng, Y. Q.; Zhang, R. Q.; Chan, K. S.; Cheung, H. F.; Lee, S. T. *Phys. Rev. B* **2002**, *66*, 045404. Feng, Y. Q.; Zhang, R. Q.; Lee, S. T. *J. Appl. Phys.* **2004**, *95*, 5729.
(24) van Houten, H.; Beenakker, C. W. J.; Staring, A. A. M. In *Single Charge Tunneling*; Grabert, H., Devoret, M. H., Eds.; Plenum Press: New York, 1992.
(25) Wang, S. D.; Sun, Z. Z.; Cue, N.; Xu, H. Q.; Wang, X. R. *Phys. Rev. B* **2002**, *65*, 125307.
(26) Tans, S. J.; Devoret, M. H.; Groeneveld, R. J. A.; Dekker, C. *Nature* **1998**, *394*, 761.
(27) Schleyer, P. V.; Maerker, C.; Dransfeld, A.; Jiao, H. J.; Hommes, N. J. R. V. *J. Am. Chem. Soc.* **1996**, *118*, 6317.